Hybrid Lead-Acid/Lithium-Ion Energy Storage System with Power-Mix Control for Light Electric Vehicles

Steven Chung, Olivier Trescases
University of Toronto
Department of Electrical and Computer Engineering
10 King's College Road, Toronto, ON, M5S 3G4, Canada

Acknowledgement

This project was supported by Polaris Industries and Brammo, Inc. The authors thank Roger Gerson, Larry Hilligoss, John Adams, Jennifer Rafiner-Jarboe, Nikita Gusev, Yueqi Chen, and Armina Khakpour for their contributions.

Keywords

≪Hybrid power integration≫, ≪Batteries≫, ≪Battery Management System (BMS)≫, ≪Energy system management≫, ≪Electric vehicle≫, ≪Power converters for EV≫

Abstract

The performance versus cost tradeoffs of a fully electric, hybrid energy storage system (HESS), using lithium-ion (LI) and lead-acid (PbA) batteries, are explored in this work for a light electric vehicle (LEV). While LI batteries typically have higher energy density, lower internal resistance and longer lifetime than PbA batteries, the module cost of LI batteries are typically three to five times the cost of PbA batteries. The objective is to design a HESS that 1) is cost-competitive with a PbA single energy storage system (SESS) and 2) maintains most of the performance benefits of a lithium SESS. A modular HESS architecture with a bi-directional dc-dc converter and controller is proposed, and a power-mix algorithm with active inter-chemistry battery state-of-charge (SOC) balancing is presented, simulated, and verified experimentally. The batteries, converter and control algorithm are modeled in MATLAB, and the effects of total ESS energy, vehicle loading, depth-of-discharge (DOD), and speed are explored. The cost and performance of the HESS are assessed side-by-side with PbA and LI single energy storage system (SESS) configurations of comparable total energy, using expected vehicle range as the performance metric. The experimental HESS has a total projected cost midway between the SESS PbA cost and the SESS Li cost, while providing 17% range and 22.5% efficiency increase over the SESS PbA vehicle.

1 Introduction

Lithium batteries have recently dominated the commercial electric vehicle (EV) landscape, while lead-acid batteries continue to play a major role in low-cost light electric vehicle (LEV), marine, and stationary electrified energy storage applications. The high cost of the lithium battery pack prevents EVs from challenging the dominance of the internal combustion engine (ICE) automobile. While current LI battery costs range from $410/kWh to >$1000/kWh, studies project that the battery powered EV will not be truly cost-competitive with ICEs until its cost falls below $150/kWh [1, 2]. Hybrid battery solutions can help bridge the cost-gap between EVs and ICEs. In the literature, hybrid energy systems for EVs typically involve ultra-capacitors or fuel cells that increase overall vehicle complexity and cost [3–6]. The deep-cycle lead-acid battery, typically one-fifth of the up-front cost of a comparable lithium-ion battery, can be paired with lithium batteries in a hybrid energy system to reduce costs.

Fig. 1: The Polaris Ranger EV.

Table I: Polaris Ranger EV specifications

Parameter	Value	Unit
Maximum speed	25	MPH
Wheel diameter	63.5	cm
Length× Width × Height	274× 143× 185	cm^3
Vehicle mass	793.8	kg
Battery bus	48	V
Battery bank energy	8.85	kWh
Maximum motor power	22.4	kW

A HESS using lithium and lead-acid batteries is proposed for a target vehicle, the Polaris Ranger EV, shown in Fig. 1. The commercial Ranger EV uses eight 12 V, 92.2 Ah lead-acid battery modules in a 4S2P (four series, two parallel) configuration, for a total vehicle 1C capacity of 8.85 kWh. The commercial vehicle specifications are shown in Table I [7]. A modified Ranger EV provided by Brammo, Inc. uses three parallel 44 V, 70 Ah Brammo lithium-ion battery modules as the energy source for a 1C capacity of 9.34 kWh. The parameters of the SESS LI and SESS PbA are detailed in Table II. Range comparisons between the two SESS vehicles show significant range and efficiency improvement in the SESS LI vehicle for a 15 MPH top speed drive-cycle compared to the SESS PbA. The performance improvements can be attributed to higher overall ESS energy and a reduction in vehicle mass, which also allows for increased vehicle payloads. The goal of this work is to develop a cost-competitive HESS that maintains most of the performance benefits of the full LI configuration with lower vehicle mass than a SESS PbA configuration.

An intelligent hybrid battery manager (IHBM), consisting of a dc-dc converter and controller, is developed to manage the power-mix and active SOC balancing between the two battery chemistries. The paper is organized as follows. Drive-cycle data collection, battery modeling, and the HESS architecture are discussed in Section 2. The power-mix algorithm and simulation results are presented in Section 3 and Section 4, respectively. Finally, the experimental results with a single IHBM are presented in Section 5.

2 Energy Storage System Modeling and IHBM Architecture

The proposed HESS topology uses four 11.2 V, 90 Ah, lithium batteries in series to make up a 45 V bus. A 12 V, 92 Ah, lead-acid battery augments each LI battery through a bi-directional dc-dc converter for a stackable, modular design, as shown in Fig. 2. The LI modules absorb the high frequency components of bus current that exist due to vehicle and inverter dynamics. A detailed block diagram of the single IHBM module is shown in Fig. 3. Specifications of the two battery modules are provided in Table III.

Drive-cycle Data Collection

Drive-cycle test data was taken using the modified Ranger EV provided by Brammo, Inc. Drive-cycle measurement results are used to accurately design the HESS architecture, to size the dc-dc converters, to validate battery and vehicle MATLAB models, and to develop the power-mix and active balancing algorithm. Each LI battery has a built-in battery management system that measures battery voltage, current, temperature and SOC, and handles fault conditions in real time. The bus current and voltage, I_{bus} and V_{bus}, respectively, are recorded to explore vehicle dynamics under various load conditions. The drive-cycle testing on the SESS LI is conducted at three load levels:

1. No load, an unloaded SESS LI LEV,
2. 140 kg load, which represents vehicle weight of a HESS LEV, and
3. 226 kg load, which represents vehicle weight of a SESS PbA LEV.

The driver adds a 78 kg load to all three test cases. The inverter bus power, P_{bus}, is shown for a zero to 15 MPH, 25 second straightaway drive-cycle in Fig. 4. Measurements for several more drive-cycles

Table II: SESS PbA, SESS LI Parameters and Normalized Range Measurements

Parameter	SESS PbA	SESS LI	Unit
Total vehicle mass including ESS	777.9	547.0	kg
Total ESS 1C energy	8.85	9.3	kWh
Total ESS specific energy	28.4	129.1	Wh/kg
Total ESS energy density	10.09	179.7	Wh/L
Unloaded range (measured)	1	1.47	p.u.
226kg loaded range (measured)	0.91	1.23	p.u.
Unloaded efficiency (measured)	1	1.40	p.u.
226kg loaded efficiency (measured)	0.91	1.17	p.u.

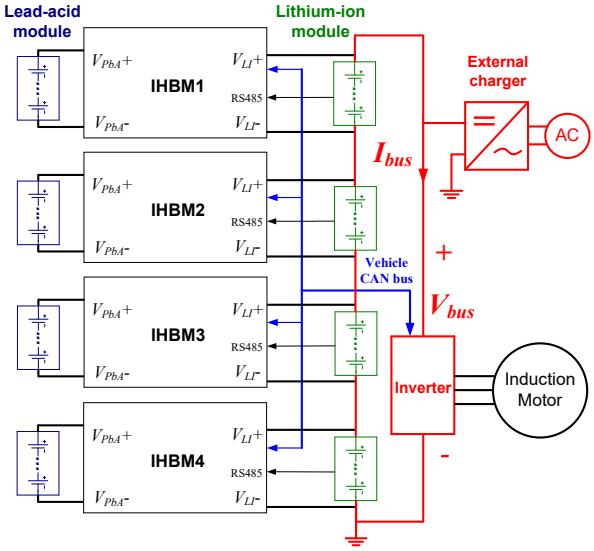

Fig. 2: Proposed HESS vehicle architecture with four modular IHBMs.

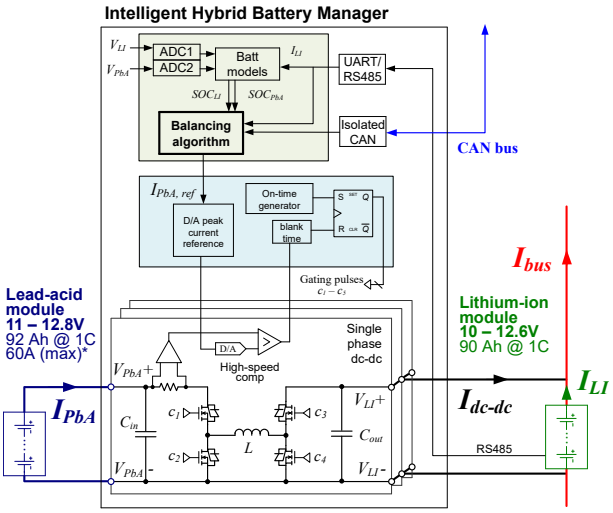

Fig. 3: Proposed IHBM architecture and modular IHBM test setup that includes an electronic load programmed with drive-cycle load profile.

were taken with various loading conditions and used for vehicle and battery modeling. The relationship between vehicle mass and load power is experimentally investigated by varying the vehicle load.

Battery Modeling

The specifications of the two chosen battery modules are given in Table III. The approximate battery costs are provided by Brammo, Inc. In the MATLAB battery models, voltage is estimated using an equivalent R-C circuit model of the battery cells [8, 9]. Battery state-of-charge (SOC) is estimated 1) from open circuit voltage (OCV) as an initial condition, and 2) by using the Coulomb counting method,

$$SOC_{batt}(k) = 100 \cdot \frac{Q_{act}(k) - Q_{batt}(k) \cdot \eta_{batt}}{Q_{act}(k)},$$
$$Q_{act}(k) = Q_{max} - \sum_{k=1}^{\infty} Q_{waste}(k), \tag{1}$$

such that Q_{batt}(k) is the discrete integral of battery current. The term Q_{act}(k) represents the total usable battery capacity, such that Q_{max} is the maximum available capacity and Q_{waste}(k) represents the amount of wasted charge due to the Peukert effect curve, depicted in Fig. 5 for the PbA module [10]. The Peukert effect of the lead-acid module is of high importance to this work, and will be revisited in the power-mix

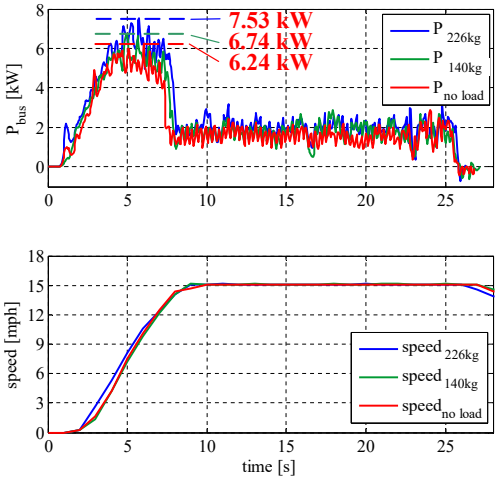

Fig. 4: Measured vehicle bus power during acceleration from 0 to 15 MPH on a straight, flat course.

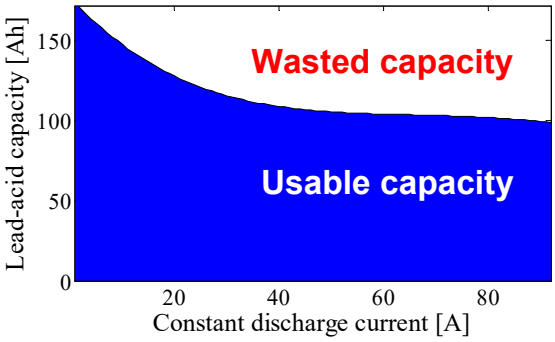

Fig. 5: Lead-acid battery capacity versus discharge current due to the Peukert effect [10].

algorithm description. The Coulomb counting method is simple to implement, but susceptible to drift over large periods of time. More robust and computationally expensive SOC estimation methods include the use of Extended Kalman Filters (EKFs) that require solving the partial differential equations of a circuit-based battery model [8, 9]. Implementation of such methods are outside the scope of this work.

The battery model is validated with measured drive-cycle data, and the modeled bus voltage and battery SOC tracks the measured values within 1 V, and within 1%, respectively, as shown in Fig. 6. The specific gravity of the PbA cells is measured to validate PbA module SOC estimation.

HESS Architecture

The proposed topology, shown in Fig. 3, is a partial power processing topology, as only a fraction of the total HESS power flows through the converter. The current flow in the inverter bus is governed by

$$\begin{aligned} I_{bus} &= I_{LI} + I_{dc-dc}, \\ I_{PbA} &= \frac{V_{LI} \cdot I_{dc-dc}}{V_{PbA} \cdot \eta}, \end{aligned} \tag{2}$$

where I_{LI} is LI current, I_{dc-dc} is dc-dc converter output current, and I_{PbA} is PbA current. V_{LI} and V_{PbA} represent LI and PbA battery voltages, respectively, and η is the converter efficiency. By controlling I_{PbA}, the currents I_{dc-dc} and I_{LI} are affected, allowing indirect, active SOC balancing.

The Peukert effect and battery voltage sag are two key lead-acid battery characteristics that dictate the dc-dc converter design. The Peukert effect influences the operating range of I_{PbA} and I_{dc-dc}, while voltage sag mandates that the converter must be able to buck or boost voltage. A non-inverting buck-boost (NIBB) topology is chosen to allow buck and boost capability, as well as bi-directional power transfer between the two battery chemistries [11].

The NIBB converter operates in peak current-mode-control with a digital current reference for tight current control. The inductor current, i_L, is detected by sensing voltage across the high-side sense resistor R_{sense}. The current in R_{sense} tracks i_L for the period when c_1 and c_3 conduct. A multi-phase, dc-dc converter approach is chosen to spread the converter hot-spots and to flatten the efficiency curve over the load range. The three, 200 W, parallel phases can be enabled depending on load, commonly referred to as phase-shedding [12, 13]. Heat-sinks are placed on the back side of the power-stage PCBs to draw heat away from the switching elements.

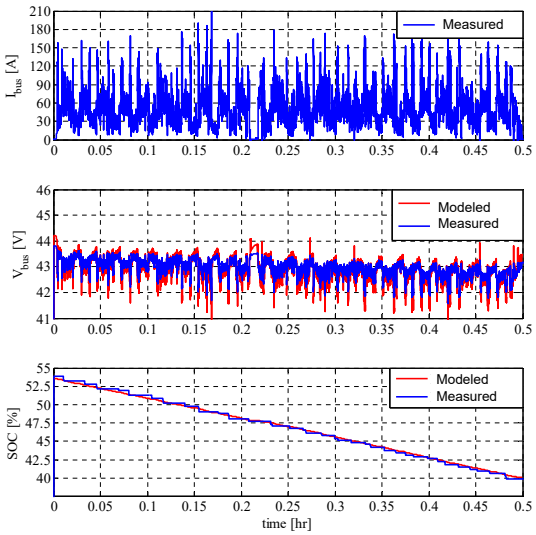

Fig. 6: Measured voltage and SOC versus modeled voltage and SOC on flat, dry asphalt and a maximum speed of 15 MPH.

Table III: LI Module and PbA Module Specifications

Parameter	LI	PbA	Unit
Nominal voltage	11.1	12	V
Voltage range	10-12.4	11-12.8	V
Capacity (1C rate)	90	92	Ah
Energy (1C rate)	1.0	1.1	kWh
Mass	8.5	39	kg
Volume	7.6	17.1	L
Specific energy	117.3	28.4	Wh/kg
Energy density	132.1	64.6	Wh/L
Cycles (80% DOD)	2000	675	
Approx. cost per kWh	900	160	$/kWh

3 IHBM Algorithm

The IHBM controller's objective is to control I_{PbA} such to maximize battery capacity utilization for any drive-cycle. This is accomplished by limiting I_{PbA} to minimize the wasted capacity quantified in (1), and illustrated as the unshaded region in Fig. 5. For example, with a constant 24 A, 0.26C discharge, the lead-acid module can provide 122 Ah of capacity, a 33% increase from the 92 Ah, 1C discharge rate capacity. The proposed HESS architecture shields the PbA battery from factors such as high acceleration events, variations in terrain, and driver aggressiveness. As such, the lead-acid SOC and energy output can be more easily controlled and tracked.

The lithium module exhibits a drop in capacity above 3C rate discharge currents. Because the drive-cycle data shows that the typical load currents for the LI do not reach this 3C discharge rate, the optimization algorithm focuses on minimizing lead-acid current to maximize the usable HESS capacity. When SOC_{PbA} reaches $SOC_{PbA,min}$, the IHBM shuts off the dc-dc converters. The ESS reaches end-of-life when $SOC_{LI,min}$ is reached, regardless of SOC_{PbA}, due to the dc-dc converter maximum power limitation. Unless otherwise stated, $SOC_{PbA,min}$ is 20%, and $SOC_{LI,min}$ is 10%.

The relative HESS SOC can take several paths from full charge, as shown in Fig. 7. The highest efficiency path is achieved when battery SOCs reach their respective minimum values while maintaining the lowest average lead-acid current. A less efficient path occurs when SOC_{PbA} reaches its minimum value before the lithium battery reaches $SOC_{LI,min}$ because the lead-acid battery is discharged at a higher rate than necessary. In this scenario, more PbA capacity is wasted due to the Peukert effect, and more energy is lost in the IHBM due to converter inefficiencies. The least efficient outcome occurs when $SOC_{LI,min}$ is reached before $SOC_{PbA,min}$ is reached because there is remaining capacity in the PbA module, resulting in under-utilization of the ESS.

The variable-step perturb-and-observe algorithm, typically used for solar maximum-power-point-tracking (MPPT), can be used to handle the SOC balancing algorithm [14–17]. The algorithm perturbs the value of I_{PbA}, and observes the resulting change in relative SOC, as illustrated in Fig. 8. The variable ΔSOC is defined as the difference between SOC_{PbA} and SOC_{Li}. ΔSOC is compared to ΔSOC_{target}, which represents the desired relative discharge path ΔSOC, and this difference is defined as err_{SOC}. By minimizing err_{SOC}, maximum energy utilization can be achieved. The perturb-and-observe method is straightforward and inherently adapts to varying vehicle load conditions. Series HESS module balancing is outside the scope of this paper.

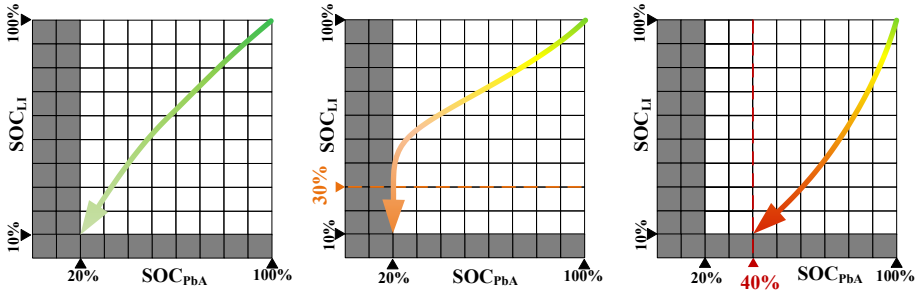

Fig. 7: From right to left, the ideal path, a less efficient path, and an undesirable path.

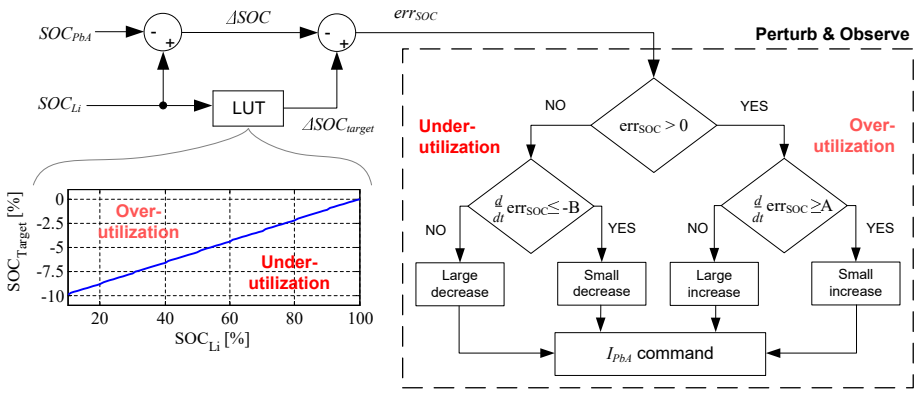

Fig. 8: Block diagram of err_{SOC} computation and perturb-and-observe algorithm.

4 Simulation Results

The effect of vehicle mass, speed, and battery DOD were simulated for the various energy storage systems. Since total available battery energy is vital to the ESS performance, two hybrid configurations of varying total ESS energy, HESS-1 and HESS-2, are considered. SESS LI-1 and SESS LI-2 are comparable full lithium configurations, respectively, in terms of total energy. The various ESS configuration parameters are detailed in Table IV. The vehicle range was simulated in MATLAB based on the measured drive-cycle conditions. The battery models are discharged from a 100% SOC initial condition to their respective minimum SOC values. Series balancing of HESS modules is assumed.

To validate the vehicle and battery models, the simulation results are compared with measured SESS results from Table II. The drive-cycle, for each measured and simulation run, is a near constant 15 MPH drive on a flat surface. For proper comparison, the range estimates of the various ESS are normalized to the SESS PbA unloaded drive-cycle, as shown in Fig. 9(a). The results show range improvements in all SESS LI and HESS configurations compared to the SESS PbA configuration, with the degree of range increase related to total ESS energy and total vehicle mass of the various configurations. The miles per ESS kWh efficiency of the various configurations are shown in Fig. 9(b). The HESS-1 has a 35% increase in estimated range with a 9.7% increase in pack energy from the SESS PbA. Meanwhile, the HESS-2 has a 17% increase in estimated range with a 5% reduction in pack energy from the SESS PbA. The two HESS configurations both have 22% increase in efficiency over the SESS PbA.

The measured SESS drive-cycle values of normalized range are in close accord with the simulated values for both unloaded and loaded conditions, with a slight mismatches due to difference in terrain between available drive-cycles. Because the expected life cycles of the lithium batteries exceeds the expected life cycles of lead-acid batteries, an additional recurring cost of replacing the lead-acid battery must be taken into account [18, 19]. The expected life-cycles of both battery chemistries are derived from datasheet parameters of depth-of-discharge (DOD) versus cycle life. The total calculated ESS costs assume a minimum of 1900 cycles to match the expected life-cycles of a single LI module. The costs amount

Table IV: Comparison of Simulated ESS Configuration

Parameter	SESS PbA	SESS LI-1	SESS LI-2	HESS-1	HESS-2	Unit
1C energy	8.85	9.34	8.06	9.71	8.45	kWh
ESS mass	312.0	82.4	68	197.2	190.0	kg
Lithium energy ratio, E_{Li}/E_{ESS}	0.00	1.00	1.00	0.545	0.486	
Unloaded range	1.00	1.50	1.27	1.35	1.17	p.u.
Unloaded efficiency	1.00	1.42	1.40	1.23	1.23	p.u.

to two PbA battery replacements to a single lithium module for any ESS. The reduction in range of operating near the PbA battery end-of-life is not considered in this work.

The Effect of Vehicle Loading

The effect of adding additional mass to the LEV is explored by simulating three loading conditions: no load, 112 kg load, and 226 kg load. The simulated range of the various ESS are normalized to the SESS PbA unloaded range, as shown in Fig. 9(a). More overall energy leads to higher range estimates for the ESS-1 cases compared to the ESS-2 cases.

The Effect of DOD on Performance and Total HESS Cost

To explore the tradeoff between life-cycle, overall HESS cost, and expected range of a given cycle, the DOD of the lead-acid battery is varied from 80% for the HESS-2 and SESS LI-2 cases. With 60% DOD, the lead-acid battery yields 950 cycles, and only one replacement PbA is necessary to achieve 1900 life-cycles for the HESS. With less usable energy, however, the range of the HESS is dramatically decreased, as shown in Fig. 10. A similar decrease in range is seen with 70% DOD. In this comparison, 80% DOD is used for the SESS PbA lead-acid batteries.

The Effect of Vehicle Speed on Range

A near constant, 15 MPH drive-cycle has been used thus far. When reducing the maximum speed by 1/3 to 10 MPH, the performance benefits of using LI batteries is diminished, as shown in Fig. 11. With a less demanding drive-cycle, the impact of the Peukert effect is less apparent. There are still modest range improvements in the HESS-2 and SESS LI-2 configurations compared to the SESS PbA due to lower overall vehicle mass.

5 Experimental Results

The experimental multi-phase dc-dc and controller are shown in Fig. 13(a), and the two battery modules are shown in Fig. 13(b). A single dc-dc phase operates with peak 90% efficiency processing 7.5 A current, and 87.5% efficiency processing 11 A current. Each phase is implemented on a single PCB with off-the-shelf discrete components. A programmable electronic-load is connected across the LI module. There are two control targets within the IHBM: 1) an FPGA, and 2) a micro-controller (MCU), which are implemented on a separate controller PCB that is common to the three dc-dc phases. The FPGA manages the high-speed converter switching operation, while the MCU handles the battery-level energy power-mix. The MCU captures salient HESS parameters such as battery voltage and current, collects the LI module parameters reported in its BMS, calculates PbA SOC, and logs the data to a computer. Forced-air cooling is used to keep MOSFET and inductor temperatures below 100^{o} C. The experimental setup resembles the HESS-2 configuration.

The HESS is tested with a 10 MPH drive for a full discharge cycle with two of three dc-dc phases, and the results are compared to the measured SESS results and to the ESS simulation results, as shown in Fig. 12. The estimated range for the measured HESS is below the straight line drawn between SESS configurations because a lower speed drive-cycle is used, as expected from the simulation result of Fig. 11. The measured SOC estimation is in agreement with the simulation results to within 5% for the

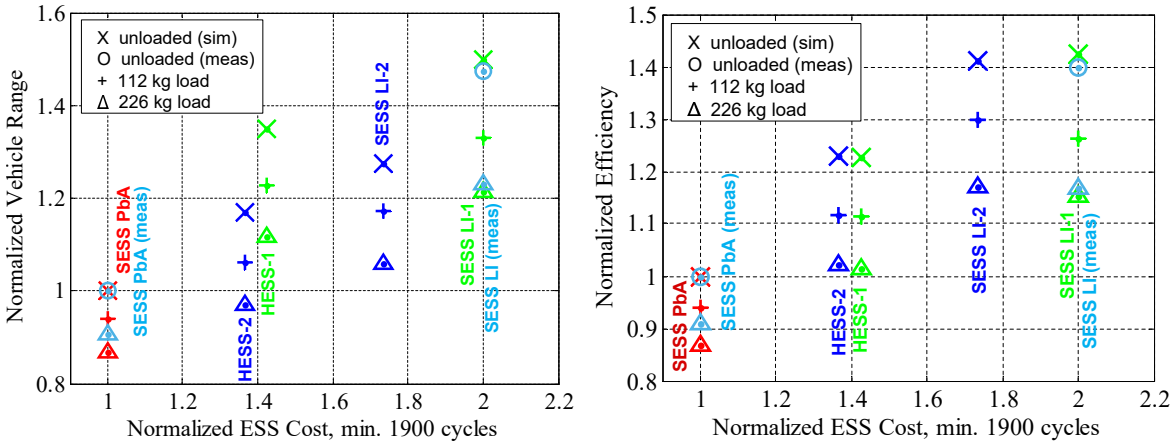

Fig. 9: Simulated vehicle (a) range, and (b) efficiency versus cost of measured SESS and simulated ESS vehicles, normalized to the no-load SESS PbA.

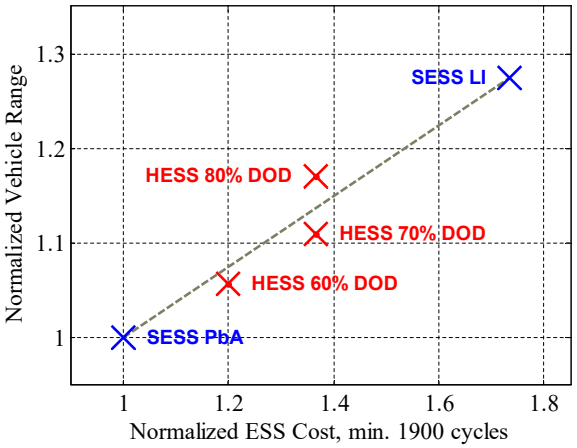

Fig. 10: The effect of HESS DOD on simulated range and cost.

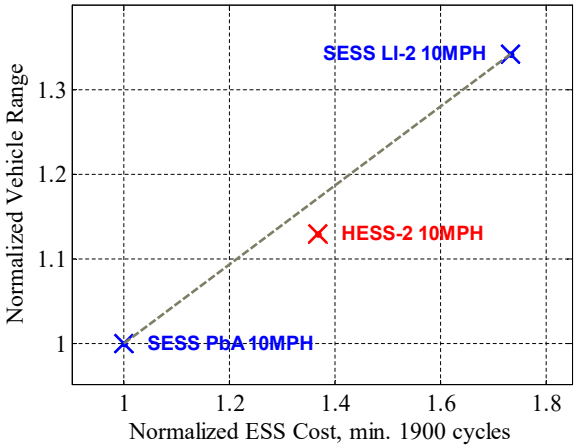

Fig. 11: The effect of slower speed and total pack energy on simulated range and cost.

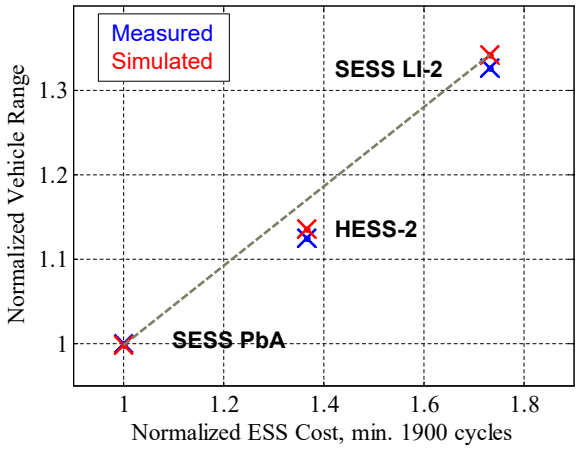

Fig. 12: The estimated range of the measured HESS and SESS configurations for a 10 MPH drive-cycle compared to simulated values.

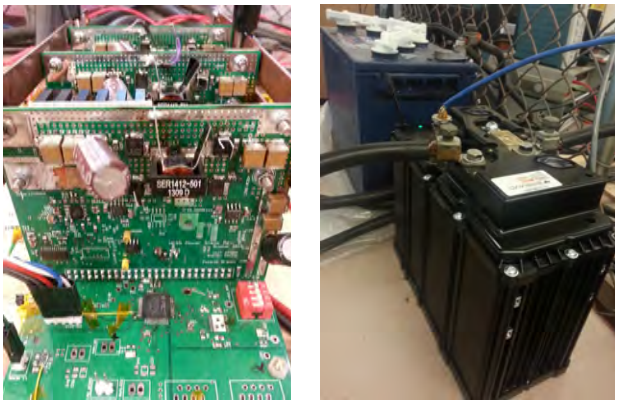

(a) (b)

Fig. 13: The (a) three dc-dc phases plugged into a common controller board and connected to battery terminal bus bars, and (b) the lithium and lead-acid batteries used for experimental verification.

duration of the experiment. The measured results show a 13% range improvement for this drive-cycle even with a 5% reduction in total pack energy from an SESS PbA. The lead-acid module SOC estimation is verified by measuring specific gravity of the cells after at minimum 4 hours of inactivity. Because the capacity fade over lifetime of the lead-acid batteries is not considered in the modeling, the estimated SOC_{PbA}, and estimated range, is slightly skewed from SOC derived from the measured specific gravity. The skew is easily corrected in the model by adjusting the total overall usable capacity of the lead-acid battery. Future work will involve paralleling all three phases of the multi-phase dc-dc.

6 Conclusions

A hybrid battery chemistry HESS using a lead-acid battery, a lithium battery, a multi-phase dc-dc converter and controller is designed, simulated, and experimentally tested in this work. The measured results show close accord of voltage, current and estimated SOC with simulated battery and system models for a 10 MPH drive-cycle, which is used to validate the simulation results. The proposed HESS achieves a 17% range improvement and 22% efficiency improvement for a 15 MPH drive-cycle, and a 13% range improvement for a 10 MPH drive-cycle, all with a 5% reduction in total pack energy from the SESS PbA vehicle. The HESS cost is estimated to be midway between the lithium SESS and lead-acid SESS configurations. Future work will involve testing the converter with all three dc-dc phases to test heavier drive-cycles.

References

[1] U. EIA, "Annual energy outlook 2013," *US Energy Information Administration, Washington, DC*, 2013.

[2] B. Nykvist and M. Nilsson, "Rapidly falling costs of battery packs for electric vehicles," *Nature Clim. Change*, vol. 5, no. 4, pp. 329–332, Apr 2015, letter. [Online]. Available: http://dx.doi.org/10.1038/nclimate2564

[3] M. Moshirvaziri, C. Malherbe, A. Moshirvaziri, and O. Trescases, "Power-mix optimization for a hybrid ultracapacitor/battery pack in an electric vehicle using real-time gps data," in *Industrial Electronics Society, IECON 2013 - 39th Annual Conference of the IEEE*, Nov 2013, pp. 4666–4671.

[4] L. Shao, M. Moshirvaziri, C. Malherbe, A. Moshirvaziri, A. Eski, S. Dallas, F. Hurzook, and O. Trescases, "Ultracapacitor/battery hybrid energy storage system with real-time power-mix control validated experimentally in a custom electric vehicle," in *Applied Power Electronics Conference and Exposition (APEC), 2015 IEEE*, March 2015, pp. 1331–1336.

[5] S. Aso, M. Kizaki, and Y. Nonobe, "Development of fuel cell hybrid vehicles in toyota," in *Power Conversion Conference - Nagoya, 2007. PCC '07*, April 2007, pp. 1606–1611.

[6] M. Jain, C. Desai, N. Kharma, and S. Williamson, "Optimal powertrain component sizing of a fuel cell plug-in hybrid electric vehicle using multi-objective genetic algorithm," in *Industrial Electronics, 2009. IECON '09. 35th Annual Conference of IEEE*, Nov 2009, pp. 3741–3746.

[7] P. Industries, "Polaris ranger ev owner's manual," 2010. [Online]. Available: $http://cdn.polarisindustries.com/polaris/common/parts-manuals/9922614r03.pdf$

[8] N. Watrin, R. Roche, H. Ostermann, B. Blunier, and A. Miraoui, "Multiphysical lithium-based battery model for use in state-of-charge determination," *Vehicular Technology, IEEE Transactions on*, vol. 61, no. 8, pp. 3420–3429, Oct 2012.

[9] R. Yamin and A. Rachid, "Modeling and simulation of a lead-acid battery packs in matlab/simulink: Parameters identification using extended kalman filter algorithm," in *Computer Modelling and Simulation (UKSim), 2014 UKSim-AMSS 16th International Conference on*, March 2014, pp. 363–368.

[10] U. Battery, "Us battery product datasheet," 2013. [Online]. Available: $http://usbattery.com/wp-content/uploads/2015/01/usb\_12V\_data\_sheet\_2015\_web.pdf$

[11] N. Mukherjee and D. Strickland, "Analysis and comparative study of different converter modes in modular second-life hybrid battery energy storage systems," *IEEE Journal of Emerging and Selected Topics in Power Electronics*, vol. 4, no. 2, pp. 547–563, June 2016.

[12] A. Costabeber, P. Mattavelli, and S. Saggini, "Digital time-optimal phase shedding in multiphase buck converters," *Power Electronics, IEEE Transactions on*, vol. 25, no. 9, pp. 2242–2247, Sept 2010.

[13] J.-T. Su and C.-W. Liu, "A novel phase-shedding control scheme for improved light load efficiency of multiphase interleaved dc-dc converters," *Power Electronics, IEEE Transactions on*, vol. 28, no. 10, pp. 4742–4752, Oct 2013.

[14] N. Femia, G. Petrone, G. Spagnuolo, and M. Vitelli, "Optimization of perturb and observe maximum power point tracking method," *IEEE Transactions on Power Electronics*, vol. 20, no. 4, pp. 963–973, July 2005.

[15] F. A. O. Aashoor and F. V. P. Robinson, "A variable step size perturb and observe algorithm for photovoltaic maximum power point tracking," in *2012 47th International Universities Power Engineering Conference (UPEC)*, Sept 2012, pp. 1–6.

[16] M. A. G. de Brito, L. Galotto, L. P. Sampaio, G. d. A. e Melo, and C. A. Canesin, "Evaluation of the main mppt techniques for photovoltaic applications," *IEEE Transactions on Industrial Electronics*, vol. 60, no. 3, pp. 1156–1167, March 2013.

[17] A. K. Abdelsalam, A. M. Massoud, S. Ahmed, and P. N. Enjeti, "High-performance adaptive perturb and observe mppt technique for photovoltaic-based microgrids," *IEEE Transactions on Power Electronics*, vol. 26, no. 4, pp. 1010–1021, April 2011.

[18] T. Dragičević, H. Pandžić, D. Škrlec, I. Kuzle, J. M. Guerrero, and D. S. Kirschen, "Capacity optimization of renewable energy sources and battery storage in an autonomous telecommunication facility," *IEEE Transactions on Sustainable Energy*, vol. 5, no. 4, pp. 1367–1378, Oct 2014.

[19] P. Poonpun and W. T. Jewell, "Analysis of the cost per kilowatt hour to store electricity," *IEEE Transactions on Energy Conversion*, vol. 23, no. 2, pp. 529–534, June 2008.